Rock Mechanics and Rock Engineering (2019) 52:4475–4496
https://doi.org/10.1007/s00603-019-01878-6

ORIGINAL PAPER

Toward a Generic Computational Approach for Flexible Rockfall Barrier Modeling

Jibril B. Coulibaly[1] · Marie-Aurélie Chanut[1] · Stéphane Lambert[2] · François Nicot[2]

Received: 13 June 2018 / Accepted: 26 May 2019 / Published online: 6 June 2019

Abstract

Flexible rockfall barriers are protection structures used to mitigate rockfall hazards in mountainous areas. The complex nonlinear mechanical behavior of these structures under impacts requires powerful modeling tools to perform structural analysis. In this article, a generic computational approach to rockfall barriers analysis is introduced. First, the generic formulation and numerical implementation in the GENEROCK software are detailed. Then, two barrier models are considered and validated against experimental full-scale tests on two different technologies. This numerical investigation permits insightful numerical investigation of the barriers' behavior. Exploratory numerical simulations are eventually performed to highlight the strengths and generality of the proposed approach. The influence of the curtain effect modeling in simulation results is presented. The effects of repeated impacts on rockfall barriers are investigated and present new insight into barrier behavior and management practices. Stochastic modeling methods are also used to study the propagation of uncertainty and variability of the structure itself in its dynamic response.

Keywords Rockfall barrier · Generic approach · GENEROCK · Curtain effect · Ring net · Stochastic modeling

List of Symbols

$\mathbf{A}$	Stochastic input variables
E	Young's modulus
E_c	Energy level
f_A	Probability density function
F_y	Activation force of energy dissipating devices
g	Earth gravitational acceleration
I	Second moment of area of post
K_1, K_2, K_3	Elastic, elastoplastic and blockage stiffness of energy dissipating devices
L	Length of post
L_{ext}	Side length of boulder
m	Mass of boulder
P_{cr}	Critical buckling load of post
P_f	Deficiency probability
R	Height ratio
r	Height ratio threshold
$\mathbf{x}^*$	Design point
$\boldsymbol{\alpha}$	Importance factor
ΔE_p	Potential energy variation
δ_s	Stroke of energy dissipating devices
Δz	Altitude variation
μ_{F_y}	Mean of activation forces
σ_{F_y}	Standard deviation of activation forces
τ	Time step
DEM	Discrete element method
FORM	First-order reliability method

✉ Jibril B. Coulibaly
jibril.coulibaly@gmail.com

Marie-Aurélie Chanut
marie-aurelie.chanut@cerema.fr

Stéphane Lambert
stephane.lambert@irstea.fr

François Nicot
francois.nicot@irstea.fr

[1] Geological Hazards Team, Cerema Centre-Est, 25 Avenue François Mitterrand, CS 92803, 69674 Bron Cedex, France

[2] Univ. Grenoble Alpes, Irstea, ETNA, 38000 Grenoble, France

1 Introduction

Infrastructures in mountainous and coastal areas may be threatened by rockfall hazards. Rockfalls are sudden events whose occurrence in time and location in space can hardly be precisely anticipated (Volkwein et al. 2011). Rockfall hazards are mitigated by means of various protection structures, such as the very efficient flexible rockfall barriers.

Such protection structures are made of several main components: an interception net, held by a set of cables, energy dissipating devices and posts, anchored to the ground. The purpose of those passive structures is to intercept the trajectory of a falling rock and to stop it before it reaches targets located downstream (Lambert and Nicot 2011). The common and developing use of rockfall barriers has raised three main research problems related to rockfall management: a scientific one, a regulatory one and an operational one. These issues are detailed in the sequel.

Understanding the mechanical response of rockfall barriers holds scientific challenges. Upon impacts, barriers exhibit a complex, non-linear, dynamic behavior. Flexibility of the structure leads to large displacements and changes in its conformation while irreversible mechanisms used to dissipate the impact energy generate localized material non-linearities. A sound understanding of barriers' structural response is necessary for design purposes. Identification of force paths, stress concentrations, weak points and failure modes would provide greater insight into the barriers' mechanical behavior.

Rockfall barriers are mainly characterized by the impact energy they can withstand known as energy level, that is, the kinetic energy of the impacting rock. Many experimental campaigns have been conducted to evaluate barriers' capacity using different procedures. Rolling rocks down a slope (McCauley et al. 1985; Smith and Duffy 1990; Duffy and Haller 1993; Andrew et al. 1998; Muraishi et al. 2005) generates realistic impacts but provides little control and repeatability over the trajectories and impact energies. Transporting boulders along a cable (Peila et al. 1998; Heiss 2004) or dropping boulders vertically (Muraishi and Sano 1999; Gerber et al. 2001; Gerber and Böll 2006; Gottardi and Govoni 2010; Bertrand et al. 2012) provides great control and reproducibility over impact conditions, but does not provide rotational velocity. The necessity to guarantee a given energy level for a barrier led to the standardization of characterization protocols (Arpin 2013). The major standard followed to justify barriers' capacity is the Guideline for European Technical Approval ETAG 27 (EOTA 2013). The ETAG 27 defines a protocol for full-scale impact testing as well as a set of performances to be met by manufacturers to be lawfully allowed to sell their products for public procurement in the European Union. The energy level of a barrier is expressed in MEL (Maximum Energy Level) and SEL (Service Energy Level). The MEL is determined by a single impact of energy E_c, centered in the central module. The SEL is determined by two successive identical impacts of energy $E_c/3$, centered in the central module. Impacts are performed with a concrete boulder of prescribed shape at a minimum speed of 25 m/s. Although a normalized protocol remains necessary, limitations in the scope of the ETAG 27 procedure have drawn interrogations regarding its representativity for more general conditions. Given the known and strong variability in rockfall events, a single loading case to which no safety coefficient is associated seems insufficient to fully justify the performances of a barrier in situ (Toe et al. 2018).

The complexity of the mechanical response of rockfall barriers bears practical challenges for manufacturers who mostly rely on empirical design procedures and need more rational and refined information to optimize their design. What is more, the necessity to perform ETAG 27 full-scale tests to certify a barrier performances generates high development costs due to the facilities and labor involved. Designing effective barriers can reduce the number of tests carried out, thereby decreasing development costs and increasing competitiveness.

To overcome these challenges and the practical shortcomings of full-scale tests, numerical modeling has been used to simulate impacts on rockfall barriers. Some researchers have developed numerical models to improve the design of some manufacturers' major technology (Nicot et al. 2001b; Volkwein 2005; Escallón et al. 2014; Gentilini et al. 2012; Bertrand et al. 2012; Castanon-Jano et al. 2018). Other models have also been used to investigate the behavior of rockfall barriers outside the scope of the ETAG 27, focusing mostly on the kinematics and shape of the incident boulder and their influence on failure mechanisms (Cazzani et al. 2002; Tran et al. 2013; Mentani et al. 2016b; Hambleton et al. 2013; Spadari et al. 2012; Bourrier et al. 2015; de Miranda et al. 2015; Mentani et al. 2016a; Toe et al. 2018). These scattered works of varying complexity mostly address the modeling of specific technologies of rockfall barriers and introduce very different mechanical assumptions and formulations. Therefore, making comparisons and drawing general conclusions remains difficult and establishing a general numerical framework with capacity to jointly answer the scientific, regulatory and operational issues appears both necessary and innovative.

In this context, the present article introduces a generic approach for modeling flexible rockfall barriers and discusses the potential use and capabilities of that approach. The principles of that generic approach are first defined and the implementation of the specifically developed GENEROCK software is detailed. General assumptions regarding barrier modeling are given and the specific barrier component models implemented and used for the present work are recalled. Validation of the assembled barrier models against several experimental full-scale impact tests on different technologies of rockfall barriers is then presented. Finally, exploratory simulations are carried out to highlight some advantages of the developed models and proposed generic approach and its ability to jointly provide answers to the scientific, regulatory and operational research problems. Modeling of the curtain effect using different assumptions is conducted and shows the importance of properly

accounting for this phenomenon in numerical simulations. Influence of boulder removal on the barrier response and effects of repeated impacts are investigated and provide original insight into barrier maintenance and management strategies for actual rockfall events. Stochastic modeling is performed to account for the variability in the behavior of energy dissipating devices.

2 Rockfall Barriers Modeling

A novel and generic numerical framework has been developed for rockfall barriers' mechanical analysis. The approach and the numerical implementation are detailed in the sequel.

2.1 Generic Numerical Approach

2.1.1 Principles and Methods

Several numerical models have been developed and used to model the response of rockfall barriers under impacts over the past decades. Many of these models have been developed to support manufacturers' economic purposes and were dedicated to rationalizing the design of their major technology. This approach often led to growth of numerical models following an identical trend: 1 manufacturer–1 technology–1 model–1 code (Table 1).

Comparison between the different barriers technologies is difficult because a model developed for a given technology 'A' may not be able to properly model another technology 'B'. Development of a generic approach for rockfall barriers' numerical modeling was pioneered by Chanut et al. (2012) in order to provide a common frame of reference for barriers' modeling and to harmonize calculation methods. That approach ambitions to:

- define a common geometric and mechanical description of all barrier technologies;
- build a unified and efficient calculation platform enabling numerical simulation of rockfall dynamic loading.

The generic approach thus defined would allow modeling and simulation of rockfall barriers under desired conditions, providing a better understanding of their behavior during controlled experiments as well as during actual rockfall events.

Table 1 Examples of rockfall barriers' numerical approaches following the 1 manufacturer–1 technology–1 model–1 code approach

Manufacturer	Model	Software
EI Montagne	Nicot et al. (2001a, b)	ECRANS
Geobrugg	Grassl (2002); Grassl et al. (2002)	FARO
	Volkwein (2004, 2005)	
	Escallón et al. (2014, 2015)	Abaqus
Maccaferri	Cazzani et al. (2002)	Abaqus
	Gentilini et al. (2013)	
GTS (now NGE)	Bertrand et al. (2012)	PFC

2.1.2 Barriers' Representation

Barriers are described by their main components: the interception net, the posts, the energy dissipating devices, the cables and the anchors. These components form the common frame of any technology and setup of rockfall barriers. Every rockfall barrier can, therefore, be described by a particular arrangement of these components. Anchors, cables, energy dissipating devices and posts are considered elementary components. The net, however, is broken down into modules, themselves broken down into periodically repeated patterns. Such a representation (Fig. 1a) is considered generic as its validity is independent of the considered technology. It also permits a very general description of complex assemblies of components.

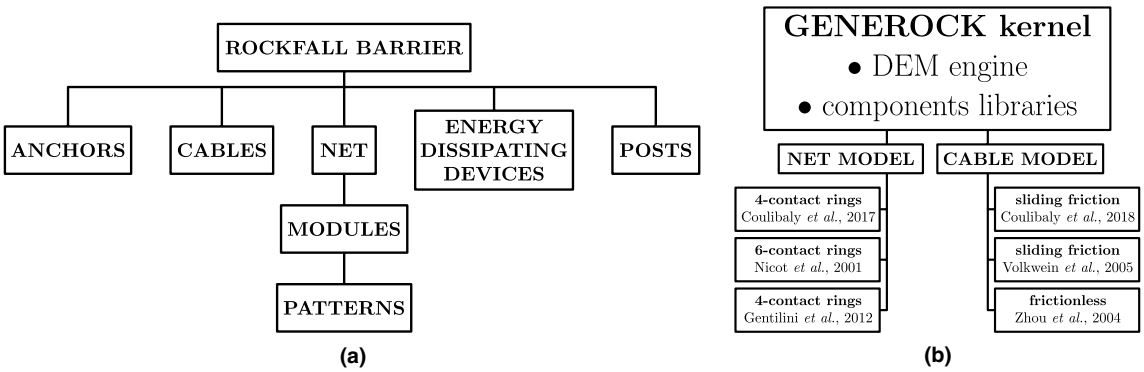

Fig. 1 Generic representation of rockfall barriers: **a** structural description, **b** software implementation and available net and cables models

2.1.3 Numerical Implementation

The numerical implementation of the previously defined generic approach is now exposed. Impact calculations are performed numerically using the GENEROCK software. This software is dedicated to rockfall barriers' modeling and simulation and uses the generic representation defined in the previous paragraph. It is based on the work of Chanut et al. (2012) and Coulibaly (2017) and is being developed by Cerema (part of the French Department of Transportation and Infrastructures). The C++ code makes use of object-oriented programming features such as classes and polymorphism to define a data structure that replicates the physical generic representation defined in Fig. 1a. Such implementation provides a unique kernel and calculation process, independent of a barrier specificity, and can easily be completed with new components and technologies without altering the fundamental code structure. Various component models, including some existing published models of cables and nets, have already been implemented in the GENEROCK software (Fig. 1b). The dynamic impact calculations are performed using an explicit Discrete Element Method (DEM). DEM models and libraries representing the main components, projectiles and their interactions are developed and used to perform numerical impacts simulations.

2.2 Mechanical Modeling of Barriers' Components

The generic approach introduced consists in a numerical tool designed and implemented to easily accommodate most barrier models. It does not, however, define any specific formulation of barrier models. The mechanical formulation remains an independent task for which many models are available in the literature. For all the components of flexible rockfall barriers identified in Sect. 2.1.2, general assumptions regarding their mechanical behavior and implementation in the GENEROCK software are first detailed. The specific formulation of the component models selected to conduct the present study are then specified.

2.2.1 Anchors

The mechanical behavior of anchors under dynamic loading is complex and requires the analysis of local soil–structure interactions. Assuming the displacement of anchors is limited and has little influence on the overall structural response, anchors are represented as fixed points in space and define Dirichlet boundary conditions of zero displacement. It is possible to account for failure of an anchor by lifting the boundary condition when a chosen rupture criterion is reached.

2.2.2 Posts

The posts are the only structural element resisting compression. In most technologies the base of the posts is hinged to the foundation although fixed based and free based, maintained by cables, can also be found. These three boundary conditions (free, hinged or fixed) are available for the base of the post. In rare case of direct impacts on posts, a deformable model accounting for plasticity is necessary. In most cases, posts undergo large displacements, especially large rotations, without necessarily sustaining large strains. Their displacements are mostly due to rigid body motion and deformations can be neglected. The latter approach is used in the present work and posts are modeled as hinged rigid bodies. Moments of inertia of the solid depend on the post material, cross-section and length. Post failure is mostly due to buckling and the rigid model allows stress analysis during the simulation to determine whether the loading of the post has surpassed its critical buckling load $P_{cr} = \pi^2 EI/L^2$.

2.2.3 Energy Dissipating Devices

Energy dissipating devices are complex systems using irreversible mechanisms such as friction, yielding and fracture to dissipate the impact energy of the boulder. The numerous and diverse existing technologies all exhibit a similar global force–displacement behavior (Castanon-Jano et al. 2017). First, the response of the device is reversible and stiff, up to the activation force. Once the activation force is reached, the irreversible mechanisms are triggered and stiffness drops. Loading maintains the irreversible mechanisms active and stiffness remains low. Depending on the technology, devices can show hardening, plastic plateau or softening when active (Castanon-Jano et al. 2017). Based on these experimental observations, energy dissipating devices are modeled as deformable one-dimensional bars with an elastoplastic linear kinematic hardening behavior (Fig. 2a). Activation force and hardening behavior can be easily controlled with few parameters: activation force F_y, elastic stiffness K_1 and elastoplastic stiffness K_2. Modeling a device with a single bar also allows for softening ($K_2 < 0$) without plastic strain localization issues. Depending on the technology, once the energy dissipating device has reached its maximum elongation, or stroke, δ_s, it can either oppose no resistance or develop increased resistance due to blockage of the dissipating mechanism with blockage stiffness K_3. Calibration parameters of the studied technologies are given in Sect. 3.

2.2.4 Ring Nets

Several technologies of nets exist: cable nets, chain-link nets, double twisted wire nets and ring nets (Volkwein et al.

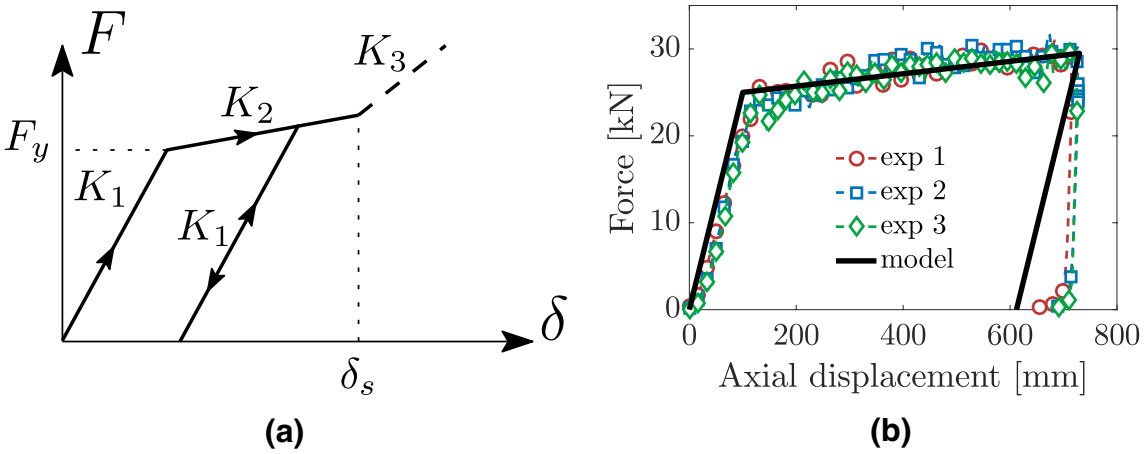

Fig. 2 Energy dissipating devices model: **a** elastoplastic behavior, **b** example of experimental response and calibrated model for barrier A

2011). They all can be described as a periodic repetition of a pattern and be implemented as such. Ring nets, made up of a repeated pattern of interlaced steel rings, are the most common and widespread type of nets. Most of the works presented in Table 1 deal with ring nets and many numerical models of such nets exist. These models range from simplified discretizations of the net pattern (Nicot et al. 2001b; Gentilini et al. 2012) to complex FEM models (Mentani et al. 2018) with three-dimensional contact interactions (Escallón et al. 2014). In the present study, barriers are modeled using a specific discrete model of steel rings developed by the authors. A summary of the model is presented in the sequel, and a complete formulation can be found in Coulibaly et al. (2017a).

The ring is discretized into 4 nodes representing the contact points with neighboring rings. The nodes interact with each other by means of 7 linear linkages: 1 perimeter, 2 diagonal and 4 side linkages (Fig. 3a). These linkages are given specific elastoplastic constitutive behaviors that account for the irreversible combined bending and tensile response of the ring under different loading configurations. The low number of discretization nodes and the use of linear linkages intend to provide both better physical accuracy than simplified models (Gentilini et al. 2012) and better computational performances than more complex 3D models (Escallón et al. 2014). 2-point traction and 4-point traction have been used as reference configurations and analytical expressions of the model response under both loading configurations were derived. A specific nonlinear multicriteria method has been developed to calibrate the model against data obtained from an extensive experimental campaign on individual rings (Fig. 3b).

Tensile tests on a 3-by-3 ring panel validate the model capacity to replicate the in-plane axial (ax) and transverse (tr) response of the assembled net. The response of the model in that configuration is nearly piece-wise linear. The initial bending and final tensile rigidities are accurately obtained, but the transition from bending to tensile behavior

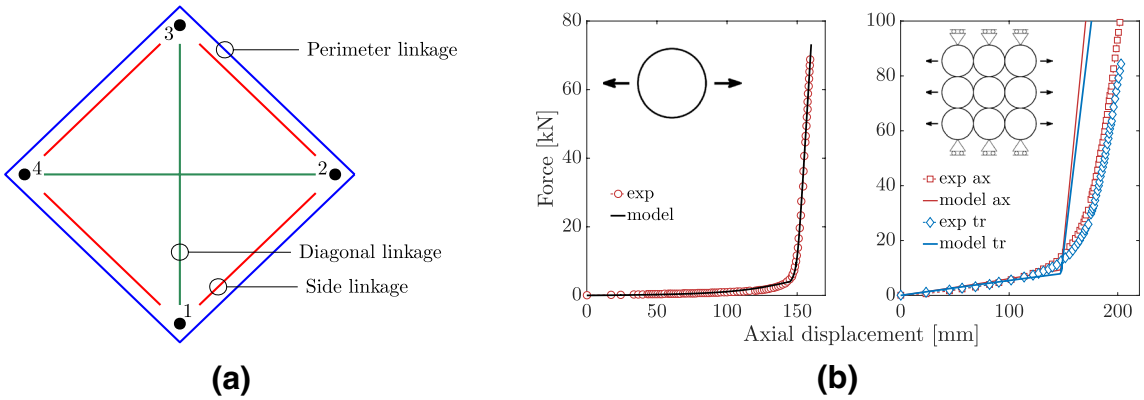

Fig. 3 Ring model: **a** discretization nodes and linkages, **b** calibration against 2-point traction experimental data (left) and validation against a 3-by-3 net panel (right) for rings of barrier A

of the ring is abrupt due to the 4-node discretization and the more constrained kinematics. The transition occurs for lower values of axial displacement in the model as also observed for other complex models, e.g. (Escallón et al. 2014). Agreement with experimental data validated the model capacity to reproduce the complex ring behavior under different loading paths and over cycles of loading and unloading (Coulibaly et al. 2017a). The ultimate strength of a single ring depends on the loading case and is smaller for the 3-by-3 panel than for the isolated ring. The maximum applied tensile force and the polygonal ring geometry upon failure are used to determine the ultimate tension along the perimeter of one ring.

2.2.5 Cables and Sliding Cables

Cables are the connection components between all the aforementioned elements. Similarly to many existing cable models, they are modeled as a succession of one-dimensional tension-only bars. In rockfall barriers, the cables supporting the net are simply woven through the rings or connected using shackles and relative sliding between the net and cables, known as curtain effect, occurs. The curtain effect introduces important changes in the geometry and it seems essential to properly account for this phenomenon in the modeling. In the present study, the barriers are modeled using a sliding cable model developed by the authors to account for relative sliding between a cable and an external element. A summary of the model is presented in the sequel, and a complete formulation can be found in Coulibaly et al. (2018).

The model consists of a multi-node sliding cable accounting for friction, with a general dynamic formulation, an effective numerical implementation and applicability to various material behaviors. First, general sliding equations are formulated and closed-form expressions of the Newton–Raphson scheme are developed to solve the sliding equations analytically. That robust mathematical formulation generalizes many existing works (Zhou et al. 2004; Volkwein 2005; Hincz 2009; Erhart 2012) and offers greater modeling capabilities. The formulation and its implementation are then validated against a theoretical dynamic sliding cable mechanism for which analytical expressions of the equation of motion and tensions are known (Fig. 4). Other models of the literature, such as (Volkwein 2005) and frictionless models (Zhou et al. 2004) have also been implemented in GENEROCK and comparison with the theoretical system demonstrates the correctness of the proposed model (Fig. 4a, b). In terms of computational efficiency, the proposed approach also surpasses existing models such as (Hincz 2009; Erhart 2012) by one order of magnitude or more (Coulibaly 2017).

3 Experimental Validation of Barrier Models

The modeling assumptions for individual components have been introduced in the previous section. Those mechanical models have been extensively studied and validated in the literature (Castanon-Jano et al. 2017; Coulibaly et al. 2017a, 2018). In the present section, complete barrier models are built by assembling those individually validated components models. Two complete rockfall barriers are modeled and validated against experimental full-scale impact tests:

- barrier A: a prototype barrier developed within the framework of the French national project C2ROP (Rockfall hazards, Protective structures and Risk mitigation) to support validation of the numerical model;
- barrier B: the CAN E barrier, a commercial barrier of 1, 500 kJ nominal capacity developed by the CAN company (CAN 2018) and certified by ETAG 27 testing.

Numerical models of these barriers are constructed and simulations of impact tests are performed and compared to the experimental results. The models' calibration is based on individual components testing; in the present work, calibration has been performed against quasi-static tests. It should be noted that differences of behavior between quasi-static

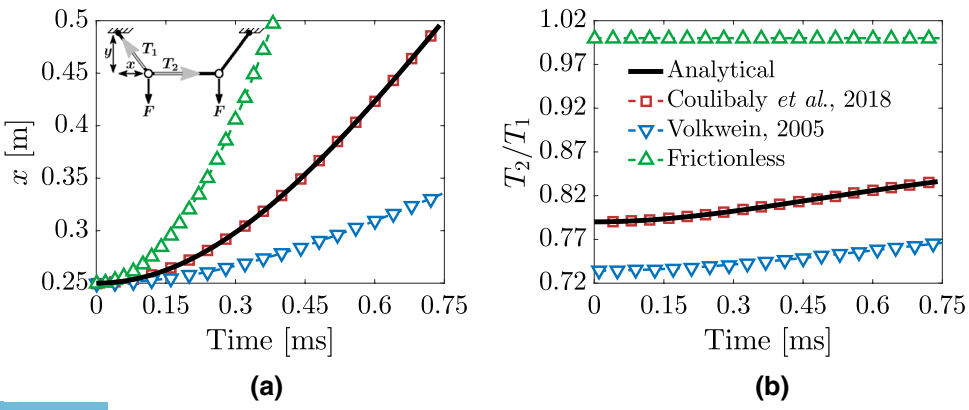

Fig. 4 Comparison between the analytical solutions and sliding cable models: **a** horizontal position of the sliding mass, **b** tension ratio around the sliding mass

and dynamic loading of the components may influence the barrier response. This is, however, not an intrinsic limitation as models can be calibrated against dynamic loading should the corresponding data become available. As opposed to several existing approaches, no back-analysis on the experimental data gathered from the full-scale tests on the entire barriers is performed. Barrier A has first been subjected to a quasi-static test to evaluate a reference energy level (Olmedo et al. 2017; Coulibaly et al. 2017b). The boulder is pulled into the net at a velocity of 0.2 m/s by a winch equipped with a force sensor. The deformation is halted at a pulling force of 225 kN and a net deflection of 5 m, corresponding to the maximum pulling force of the apparatus. The force–displacement curve of the barrier is then integrated to obtain the work energy, providing a reference energy level of the barrier of 270 kJ. No failure was observed at that level of loading; the reference energy is, therefore, a lower bound estimate of the maximum impact energy. Subsequently, a single impact test has been performed using the previously determined reference impact energy, as well as three successive impacts at 90 kJ, one third of that reference energy. Barrier B has been subjected to ETAG 27 MEL and SEL tests. For brevity, only results from the single impact full-scale test for barrier A and the ETAG 27 SEL test for barrier B are reported in this article. Exhaustive validation results for both barriers and for all the aforementioned loading cases are reported in (Coulibaly 2017). Those results demonstrate the validity of the approach for multiple technologies and different loading cases. The barrier models studied herein are ones of the very few numerical models known to the authors that have been validated against repeated successive impacts tests (Gentilini et al. 2013) and against several distinct technologies of rockfall barriers.

3.1 Single impact test on barrier A

3.1.1 Barrier Description and Components' Characterization

Barrier A is made up of four steel posts, delimiting three modules spanned by a ring net (Fig. 5a). The posts are 2.75 m tall and have a hollow circular cross-section of 89 mm outer diameter and 8 mm thickness. The 15 m long net is made up of three 5 m long modules. Each module is made of 16 alternated rows of 12 rings of diameter 275 mm. Each post is maintained by a set of 16 mm diameter cables: two upstream cables, one downstream cable and an additional lateral cable for external posts. The net is supported by a set of 12 mm diameter lower and upper longitudinal cables, each spanning two modules and by closing cables that maintain the lateral sides of the net to the external posts. Energy dissipating devices are located at both ends of every longitudinal cable. Experimental characterization of the ring net and energy dissipating devices is performed based on quasi-static tests presented in Olmedo et al. (2017). The models are calibrated against the obtained data as presented in Figs. 2b and 3b. The 14 parameters of the ring models are not recalled for brevity and can be found in Coulibaly (2017). The ultimate tension along the ring perimeter determined from the 3-by-3 test presented in Fig. 3b is 23.3 kN. The parameters of the energy dissipating devices are $F_y = 25$ kN, $K_1 = K_3 = 250$ kN/m, $K_2 = 7.15$ kN/m and $\delta_s = 2.5$ m. Cables are given an elastic linear constitutive relationship with Young's modulus of 100 GPa. The friction coefficient for the curtain effect is taken equal to 0.3 (Moon et al. 2014). The friction coefficient between the boulder and the net is chosen equal to 0.5 (Escallón and Wendeler 2013).

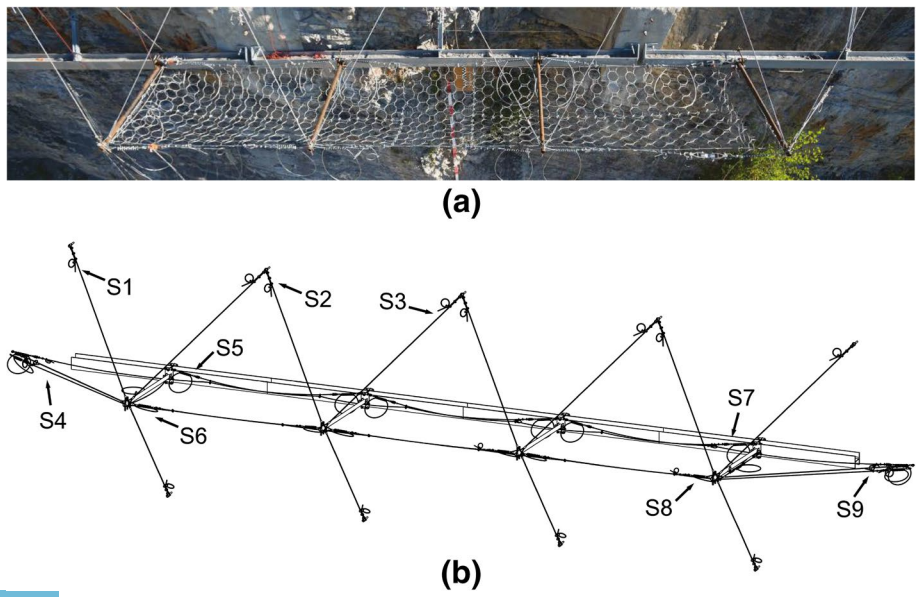

Fig. 5 Barrier A: **a** barrier installed in the testing facility of Rompon, France (source CAN), **b** locations of force sensors (source NGE)

3.1.2 Full-scale Test Description

The barrier is installed horizontally in a vertical drop testing facility (Fig. 6a). A single impact test is performed and repeated twice on two identical barriers to monitor experimental variability of the barrier response. An ETAG 27 shaped boulder of size $L_{ext} = 750$ mm and mass $m = 740$ kg impacts the center of the central module at a speed of 27 m/s, representing an impact energy of 270 kJ.

A comprehensive instrumentation is installed to monitor the barrier response. A high-speed camera is used to track the vertical trajectory of the boulder with a frequency of 500 frames/s. Upstream, lateral and longitudinal cables are equipped with axial force sensors identified in Fig. 5b.

3.1.3 Numerical Simulation Description

The impact test is simulated (Fig. 6b) as follows:

1. gravitational equilibrium (2 s);
2. impact (0.4 s);

The timestep for the explicit simulation is taken as $\tau = 10^{-5}$ s, coordinates and forces are saved with a respective frequency of 500 Hz and 10 kHz. Simulation on an Intel Core i3-4100M 2.50 GHz CPU takes 340 s (280 s for gravitational equilibrium, 60 s for impact). The time factor (simulation duration/simulated time) is around 140. In comparison, a computational time of 5 min for a 0.3-s impact phase is reported by Mentani et al. (2018) for impact simulations using Abaqus/Explicit on an Intel Xeon E3-1240 v5 3.50 GHz CPU for a chain-link barrier of similar dimensions and using the same numerical timestep. That corresponds to a time factor of about 1,000, nearly one order of magnitude larger than that of the present model. The finer chain-link net in Mentani et al. (2018) possesses about 5 times more degrees of freedom than the ring net of barrier A and may partially explain the tenfold difference in the time factor. The CPU frequency (3.50 GHz) is, however, 40% larger than the one used in the present calculation (2.50 GHz). Scaling the tenfold time factor difference to the number of degrees of freedom and CPU frequency, the computational efficiency of the proposed approach remains about twice as large as that of (Mentani et al. 2018).

3.1.4 Results and Comparison

The global and local responses of the barrier are successively investigated and the numerical solution is compared to the experimental data. Figure 7a shows the net deflection over time. Simulation results are similar to experimental data. The trend and peak values are close and the numerical curve is located between the two experimental ones; the impact test having been repeated on 2 separate barriers. It is very interesting to notice that the barrier exhibits a different response for the two experimental impact tests carried out. This points out the noticeable variability of the barrier response, likely due to small setup differences during barrier erection, and to variability in the energy dissipating devices elongation as further discussed in Sect. 4.1. This questions the suitability of model calibration through back-analysis on a single experimental test as done in Gentilini et al. (2012) and Luciani et al. (2017).

Tensions in upstream cables S1, S2 and S3 (Fig. 7b–d) as well as in symmetric lateral cables S4 and S9 (Fig. 7e) are investigated. Simulation results agree very well with experimental data. The loading duration and timing match, as well as the peak forces. These results highlight the capacity of the model to reproduce the dynamic response of the barrier and in particular, to respect the force paths, that is the stress propagation within the structure components from the impacted area to the anchors. Tension in the symmetric sensors S8 and S6 of the upper longitudinal cable (Fig. 7f) and S7 and S5 of the lower longitudinal cable (Fig. 7g), equipped with energy dissipating devices, are studied (for technical reasons, experimental results for S8 (Fig. 7f) cannot be correctly analyzed). Longitudinal cables response is governed by the energy dissipating devices response. Simulation results show good agreement with experimental data in terms of timing and activation force. The experimental

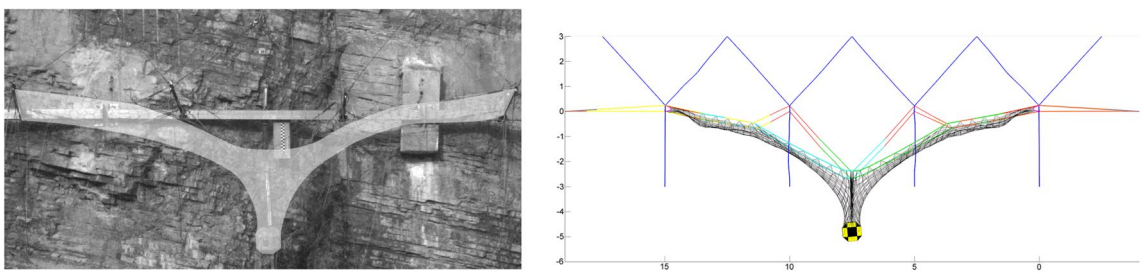

Fig. 6 Impact on barrier A: **a** full-scale test (net highlighted for better visibility), **b** numerical simulation

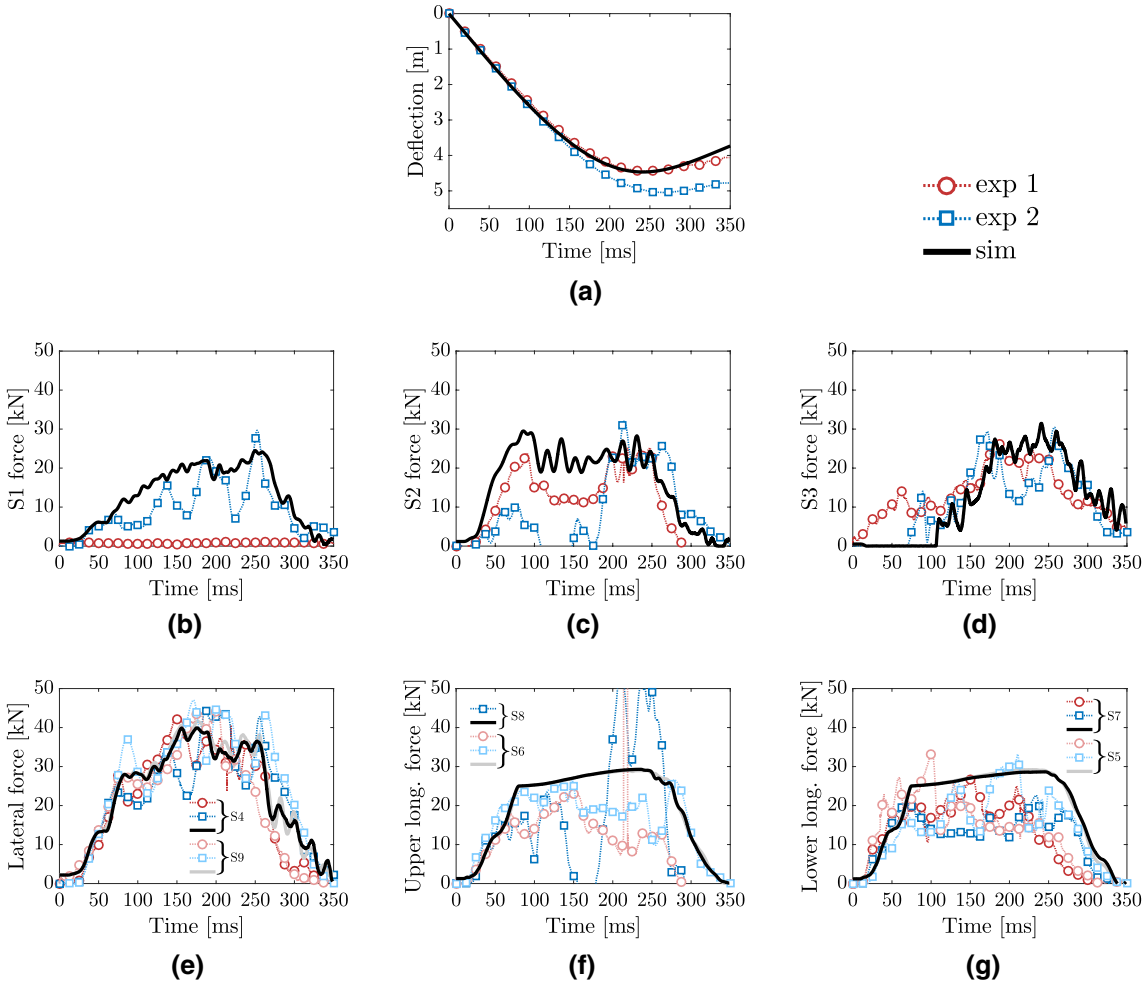

Fig. 7 Response of barrier A: **a** deflection of the barrier, **b** force in upstream cable S1, **c** S2, **d** S3, **e** force in lateral cables S9 and S4, **f** force in upper longitudinal cables S8 and S6, **g** force in lower longitudinal cables S7 and S5

dynamic response of the devices is, however, less smooth and shows less hardening than the model calibrated against the quasi-static tests and using the elastoplastic behavior presented in Fig. 2b. Both experimental measurements and numerical simulations show a rather similar response for symmetric force sensors in the structure. There is no failure of the post due to buckling. Assuming Young's modulus of 200 GPa for the steel posts, the critical buckling load is $P_{\text{cr}}^{A} = 440\,\text{kN}$. The maximum axial compressive load in the posts P1–P4 is, respectively, 97 kN, 48 kN, 47 kN and 98 kN, largely below the critical load.

3.2 SEL Impact Test on Barrier B

3.2.1 Barrier Description and Components' Characterization

Barrier B is made up of 4 steel posts, delimiting 3 modules spanned by a ring net (Fig. 8a). The posts are 4.25 m tall and have a hollow circular cross-section of 168 mm outer diameter and 4.5 mm thickness. The 30-m long net is made up of three 10 m long modules. Each module is made of 18 alternated rows of 20 rings of diameter 350 mm. Each post is maintained by a set of 20 mm diameter cables: two upstream cables and an additional lateral cable for external posts. The net is supported by a pair of lower and upper longitudinal cables, each spanning all 3 modules. An additional pair of intermediate longitudinal cables, centered in the barrier height, spans all 3 modules as well. All longitudinal cables are 16 mm in diameter. Closing cables of 12 mm in diameter also maintain the lateral sides of the net to the external posts. Energy dissipating devices are located at both ends of every pair of longitudinal cable. This barrier differs from barrier A by its cable weaving pattern, larger dimensions and smaller number of cables and energy dissipating devices. The longitudinal cables of barrier B span the entire structure, resulting in a different geometry than barrier A that influences force paths. The dissipating devices are also all positioned on the

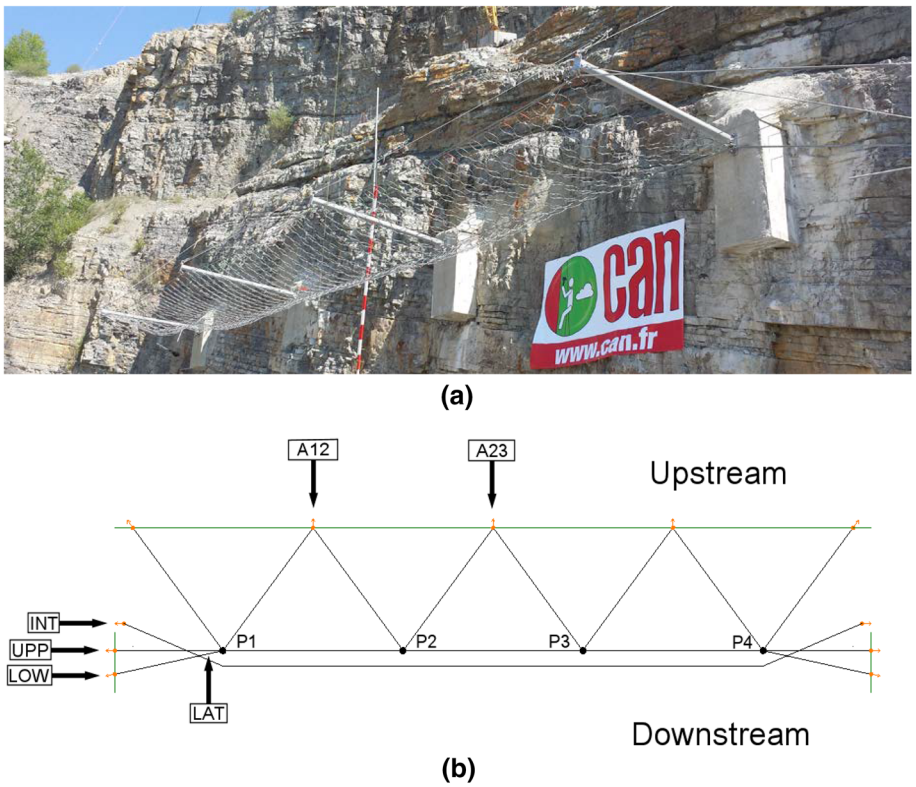

Fig. 8 Barrier B: **a** barrier installed in the testing facility of Rompon, France, **b** location of force sensors. P1–P4 represent the posts (source CAN)

external sides of the barrier, energy dissipation is, therefore, concentrated in a few locations rather than distributed throughout the structure as in barrier A. The ring net model calibration process is detailed in Coulibaly et al. (2017a). Energy dissipating devices and other components are calibrated against confidential experimental data provided by the manufacturer CAN. As for barrier A, cables are given an elastic linear constitutive relationship with Young's modulus of 100 GPa and sliding friction coefficient of 0.3 and a value of 0.5 is chosen for the friction coefficient between the boulder and the net.

3.2.2 Full-Scale Test Description

The barrier is installed horizontally in the same vertical drop testing facility as barrier A. The ETAG 27 certification SEL test is performed; it consists of two consecutive and identical centered impacts on the barrier. After the first impact, the boulder is removed and dropped again without any maintenance allowed between the two impacts. A boulder of size $L_{\text{ext}} = 920$ mm and mass $m = 1550$ kg is used to impact the center of the central module at a speed of 25.4 m/s, representing an impact energy of 500 kJ.

Similar instrumentation as for barrier A is used to monitor the barrier response: high-speed camera and axial force sensors on upstream anchors, lateral and longitudinal cables (Fig. 8b). After the boulders are stopped by the structure, elongation of the energy dissipating devices, as well as residual height (horizontal, between the upper and lower longitudinal cables) and deflection (vertical, in impact direction) are measured.

3.2.3 Numerical Simulation Description

The ETAG 27 SEL test is simulated as follows:

1. gravitational equilibrium (2 s);
2. two successive impacts with boulder removal:
   (a) impact (0.4 s),
   (b) gravitational equilibrium before boulder removal (3 s),
   (c) gravitational equilibrium after boulder removal (3 s).

The timestep for the explicit simulation is taken as $\tau = 10^{-5}$ s; coordinates and forces are saved with a respective frequency of 500 Hz and 10 kHz. Simulation on an Intel Core i3-4100M 2.50 GHz CPU takes 4455 s (595 s for initial gravitational equilibrium, 130 s for each impact and 1800 s for each post-impact equilibrium). The time factor (simulation duration/simulated time) is around 300. The time factor remains small, and the increase in calculation cost compared to barrier A is mostly due to the larger dimensions of barrier B.

3.2.4 Results and Comparison

The global and local responses of the barrier are successively investigated. Figure 9a shows the barrier deflection over time during the two impacts, noted SEL 1 and SEL 2. Deflection measurements represent the elongation of the net for each impact, not the cumulative elongation: for both impacts, deflection is zeroed at the instant the boulder comes into contact with the net. Simulation results are in good accordance with experimental data for both impacts. Clips connecting the net to longitudinal cables in the vicinity of the posts are designed to fail at a given tension to prevent damage of the net. Failure of some clips has been observed during the second impact of the experimental test. Failure of these elements has not been modeled for simplicity and may explain the stiffer response of the model during the second SEL impact.

Tensions in upstream anchors A12 and A23 (Fig. 9b, c) as well as lateral (Fig. 9d) and longitudinal cables equipped with energy dissipating devices (Fig. 9e–g) are studied. Simulation results agree well with experimental data. The loading duration and timing match, as well as the peak forces in most components. The very low numerical tension values in the lateral cable might be explained by some modeling simplifications. In the actual structure, cables are attached at different locations at the top of the external post and generate some twist which affects the load distribution among cables. The eccentricity at the top of the post has not been modeled and may explain the differences in tension with experimental data. The model finely reproduces the change in the structure behavior, with a quicker loading time, shorter loading duration and higher peak tension during the second impact than during the first one. These results highlight the validity of the mechanical modeling of the irreversible processes occurring during impact and boulder removal as the response of the barrier during the second impact depends on its state after the first one. These aspects are also validated by the geometry of the deformed barrier. Table 2 details the

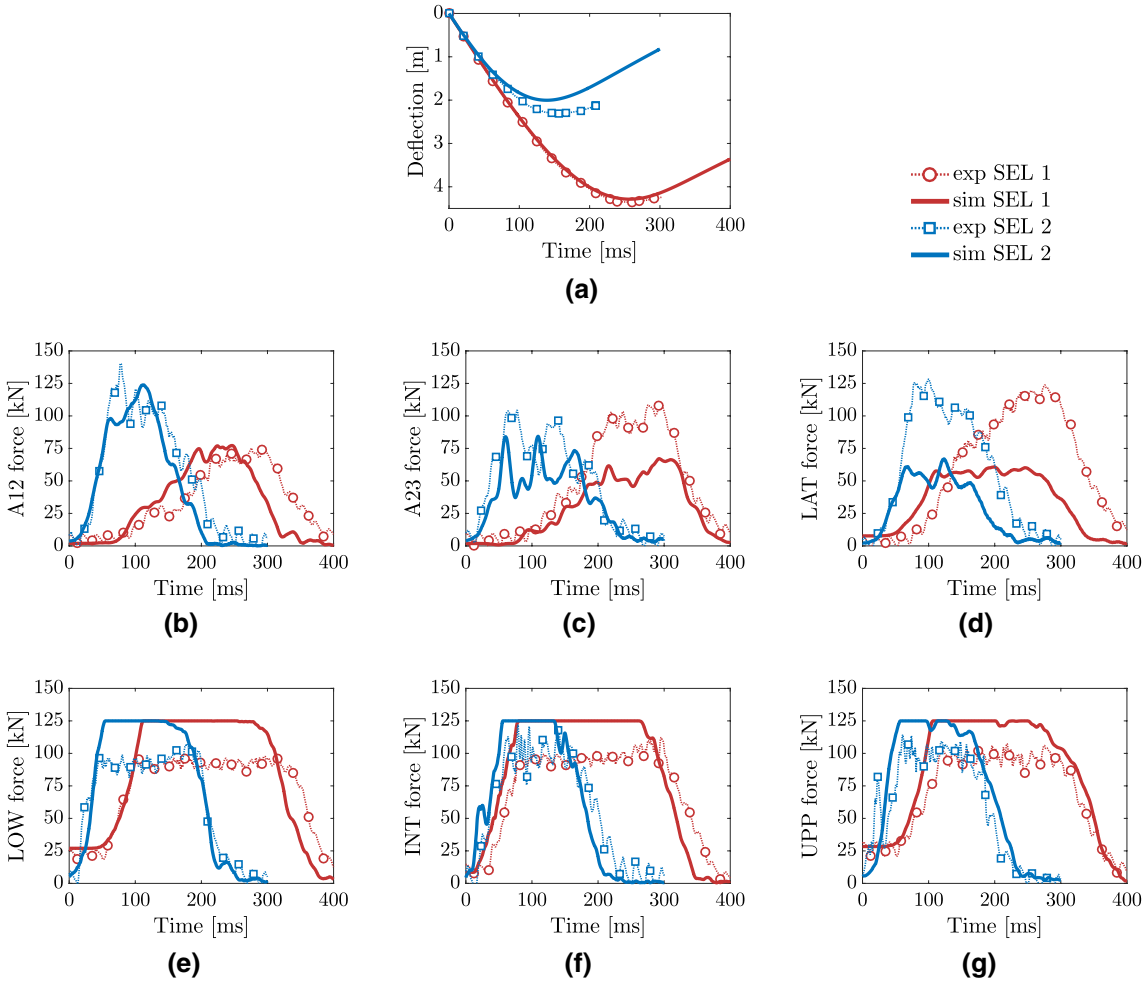

Fig. 9 Response of barrier B: **a** deflection of the barrier, **b** force in A12 upstream anchor, **c** force in A23 upstream anchor, **d** force in lateral cable, **e** force in lower longitudinal cables, **f** force in intermediate longitudinal cables, **g** force in upper longitudinal cables

Table 2 Residual deflection and residual height of barrier B after SEL test

Residual dimension	Exp (1/2) (m)	Sim (1/2) (m)	Variation (%)
Deflection (before removal)	3.71/4.52	3.56/4.29	−4.0/ − 5.1
Deflection (after removal)	2.74/3.54	2.91/3.66	+6.2/ + 3.4
Height (before removal)	2.87/2.64	3.05/2.79	+6.3/ + 5.7
Height (after removal)	3.30/3.04	3.35/3.06	+1.5/ + 0.6

residual deflection and height of the barrier before and after removal of the boulder. The numerical results obtained from simulation present less than 10 % of relative error on the residual dimensions. The critical buckling load for barrier B is $P_{cr}^{B} = 845\,\text{kN}$. The maximum axial compressive load in the posts is slightly larger during the second impact. For posts P1–P4 it is, respectively, 160 kN, 114 kN, 115 kN and 19 kN, largely below the critical load.

The numerical models of both barrier A and B have been developed and calibrated on individual component's testing and comparison with full-scale impact tests offered validation results. Further details regarding the experimental response and calibration of the components, the barriers testing and comprehensive validation results over additional loading cases can be found in Coulibaly (2017).

4 Numerical Investigation of Rockfall Barriers' Behavior

The developed generic approach along with the components' models developed makes the numerical modeling of various technologies of rockfall barriers possible and efficient. The validation carried out in the previous section highlights the validity of the individual components' models and of the two assembled barrier models introduced in the present study. On top of strong versatility, developments of the ring model (Coulibaly et al. 2017a) and sliding cable model (Coulibaly et al. 2018) have been carried out with a clear focus to finely model the curtain effect and the irreversible mechanisms undergone by the structure with a low computational cost. In this section, the benefits and potential of the barrier models and the GENEROCK software are displayed through an exploratory numerical investigation. Three particular aspects are investigated:

1. the influence of the modeling of the curtain effect on the structural response;
2. the mechanical response of the structure subject to repeated impacts;
3. the mechanical and stochastic coupling to assess structural reliability.

Thorough numerical investigation of these three aspects is, respectively, accessible thanks to:

1. the rigorous modeling of the sliding friction mechanism and curtain effect;
2. the detailed modeling of the irreversible and plastic behavior of the structure over loading/unloading phases;
3. the low computational cost of the numerical simulations.

The GENEROCK software can also be used to perform more classical simulations: varying the impact conditions (location, kinematics, volume...), modifying the structure geometry (homothety of modules dimensions, posts angles, barrier misalignment...) or preloading the structure with rubble (Chanut et al. 2018). For the purposes of this article, the authors wish to highlight some novel opportunities brought by the proposed barrier models and their implementation. The model of barrier A is chosen to perform those simulations. As a research prototype bearing no industrial or commercial interests, it is particularly well suited for this exploratory work.

4.1 Influence of the Curtain Effect Modeling Assumptions

In this section, the influence of different modeling assumptions for the curtain effect on the barrier response is investigated. Single impact simulations are performed in the conditions described in Sect. 3.1 with varying assumptions regarding the curtain effect:

- curtain effect with friction modeled with the developed sliding cable model introduced in Coulibaly et al. (2018) and presented in Sect. 2.2.5. This configuration is labeled CEF;
- curtain effect without friction. This configuration is labeled CENF;
- no curtain effect, sliding only occurs between the cables and the posts. This configuration is labeled NCE;
- no sliding, cable-net and cable-post connections are pinned. This configuration is labeled NSL.

Simulation results of the different configurations are presented in the sequel and compared to experimental results. Account of the curtain effect has a strong influence on the global response of the barrier (Fig. 10a). Simulations performed without curtain effect result in a very stiff barrier with short braking time and small deflection, between 3.4 and 3.8 m. Allowing sliding at the posts (NCE) provides more flexibility and fully accounting for the curtain

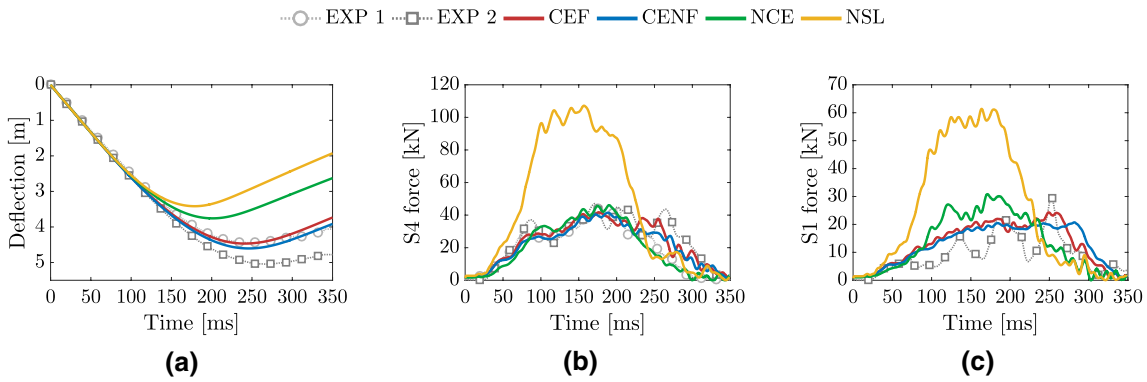

Fig. 10 Influence of the curtain effect on the response of barrier A: **a** deflection of the barrier, **b** force in lateral cable S4, **c** force in upstream cable S1

effect shows good results when compared to experimental data, with deflection around 4.5 m. Frictionless sliding (CENF) results in a more flexible barrier as no friction force opposes the curtain effect and barrier deflection. These results should be regarded with particular attention when calibration through back-analysis is involved. One strategy to account for the increase in deflection due to the curtain effect could consist in lowering the stiffness of other components of the structure, such as the net, to reach a satisfying global stiffness. Such modeling assumptions should be avoided as the local behavior of the components is not respected and could lead to discrepancies in the deformed shape and force paths. The equilibrium geometry of the barrier after impact is also strongly affected by the account of the curtain effect (Table 3). Residual deflections are smaller the more sliding is constrained. Residual height before boulder removal follows an opposite, yet expected, trend: the more sliding is constrained, the larger the residual height. Residual height after boulder removal, however, presents very surprising results: the curtain effect favors larger residual heights. When curtain effect is considered (CEF and CENF), removing the boulder leads to redistribution of the net and cables mass between the modules, leading to an increase in residual height in the central module after removal. When curtain effect is not considered (NCE and NSL), the weight is transferred to the cables and the posts instead, resulting in almost no change in the residual height before and after boulder removal (Table 3).

The local response of the barrier is also influenced by the account of the curtain effect (Fig. 10b, c). The total absence of sliding (NSL) results in extremely high forces in some cables. This is due to the existence of paths without energy dissipating device between the boulder and the anchors. When sliding is permitted at the posts, these paths disappear and tensions do not show substantial differences whether curtain effect is accounted for (CEF and CENF) or not (NCE) since tensions are mostly governed by the activation force of the energy dissipating devices. However, the force paths are altered by the account of the curtain effect. The elongation of the energy dissipating devices is monitored for the different configurations. The barrier devices are located and identified in Fig. 11a and elongations are reported in Fig. 11b. The layout of the different bar charts in this figure is chosen so as to replicate the actual layout of the devices in the barrier presented Fig. 11a.

The energy is mostly dissipated in the devices located at the ends of the cable connecting posts P1–P3 (UL1, LL1, UR2 and LR2), as well as posts P2 to P4 (UL2, LL2, UR3 and LR3) (Fig. 11b). Elongations from the two experimental tests differ drastically. For instance, the upper central devices UL2 and UR2 show very little elongation for the first test and the outer devices located on the same cables, respectively, UR3 and UL1, are strongly activated. Some devices are not activated during one test and show important elongations during the other (UL1, LEL and LR1). This variability is due to individual differences in energy dissipating devices' properties and causes uncertainty in the response

Table 3 Residual deflection and residual height of barrier A for the different curtain effect configurations

Residual dimension	Exp 1/2	CEF (m)	CENF (m)	NCE (m)	NSL (m)
Deflection (before removal)	3.97/4.58	3.84	3.98	3.21	2.67
Deflection (after removal)	3.58/3.79	3.32	3.52	2.92	2.38
Height (before removal)	1.20/1.40	1.31	1.29	1.38	1.56
Height (after removal)	1.40/–	1.73	1.69	1.40	1.60

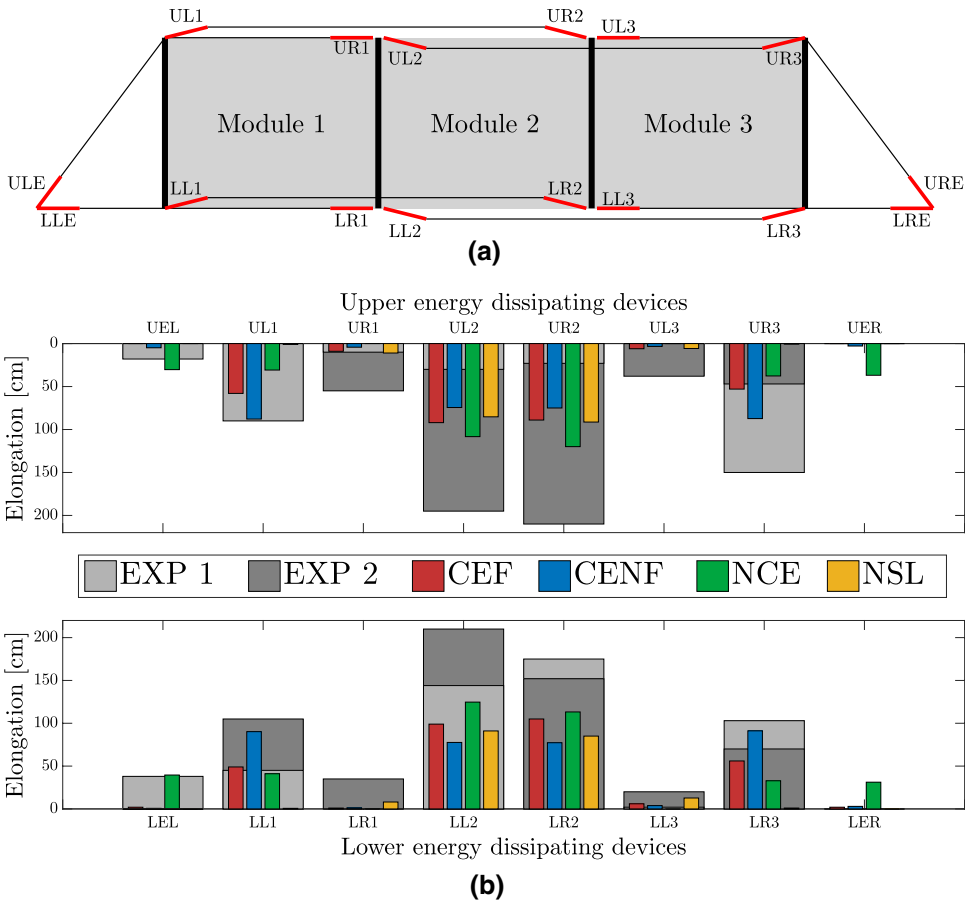

Fig. 11 Influence of the curtain effect modeling assumptions on the energy dissipating devices elongation: **a** identification and location of the energy dissipating devices of barrier A, **b** elongation of the energy dissipating devices

as previously observed with the barrier deflection. Because of the important variability in the experimental response, conclusive comparison and validation of the deterministic numerical results is not easy. From numerical simulations, dissipation concentrates in the same devices although elongations are shorter due to the larger forces in the energy dissipating devices (Fig. 7f, g). The higher force and shorter elongation obtained numerically may, however, result in similar amounts of dissipated energy than the larger elongation and smaller forces observed experimentally. When friction is taken into account (CEF), devices located on the same cable withstand different elongations. Without friction (CENF), tension is uniform along the cable and the differences are reduced. The total elongation is greater when friction is neglected (682 cm for CENF, 627 cm for CEF) since all energy must be dissipated by the devices (Coulibaly et al. 2018). Configuration NCE shows large elongation over all devices, except for those located on the outside of the central module, and the largest total elongation of all studied cases (747 cm). In the extreme case NSL, large amounts of the impact energy are stored elastically in the structure, generating high forces, as shown in Fig. 10b, c, and the smallest total elongation (393 cm) of all studied cases, mostly concentrated in the central devices.

These results illustrate the practical features of the curtain effect. By lowering the overall stiffness of the structure, the curtain effect allows for a greater deflection that has two consequences: more regions of the structures contribute to resisting the impact and, a greater fraction of the impact energy is absorbed by the structure as elastic energy. That leads to lower stress and lower use of the energy dissipating devices. The unequivocal observation of these differences in simulation results also indicates that not considering the curtain effect in numerical simulations can lead to an erroneous analysis of the global and local response of the structure. These results hold for the technology of barrier A. Depending on the barrier technology, geometry and assembly methods, neglecting the curtain effect in numerical simulations may result in other types of discrepancies.

4.2 Mechanical Response to Repeated Impacts

In this section, the numerical investigation focuses on the mechanical response of rockfall barriers under repeated impacts. Two aspects are investigated: the influence of boulder removal on a barrier response and the asymptotic response of a barrier under repeated, identical impacts. Besides the scientific interest of this study, these

developments can also provide beneficial practical and operational information regarding maintenance practices. The purpose of the first investigation is to determine whether boulder removal is influential. The second investigation completes the first one and aims to determine the asymptotic behavior of the barrier and its capacity in absence of maintenance.

4.2.1 Influence of Boulder Removal on Consecutive Impacts

The ETAG 27 SEL test consists of two consecutive impacts with boulder removal and without possible maintenance on the barrier. The philosophy behind this procedure is that in realistic conditions, it is not always possible to detect when an impact occurs and to immediately apply maintenance operations on the barrier. The barrier must, therefore, be capable of sustaining an additional impact without any maintenance performed after a first one. However, for the same reasons, it is most of the time impossible to perform tasks such as boulder removal either, and the second impact would happen while the first boulder has not been removed from the net, a case that differs from the ETAG 27 SEL procedure.

Simulations and results The two following cases are considered to analyze the influence of boulder removal:

1. successive impacts of two boulders with removal of the first boulder;
2. successive impacts of two boulders without removal of the first boulder.

Vertical drop simulations are considered in order to cancel out the potential influence of terrain–boulder interactions. The boulders are spherical, with a mass of 740 kg and diameter of 750 mm. Boulders are positioned symmetrically in the central module, 900 mm away from the middle of the barrier and 900 mm away from the top. The boulders impact the barrier at a speed of 15.6 m/s, corresponding to an impact energy of 90 kJ (Fig. 12a), one-third of the reference impact energy of the validation single impact test presented in Sect. 3.1.

Simulation results are reported for both cases, with and without boulder removal. The dynamic response of the barrier is presented in Fig. 12. The response differs between the first and second impact but little difference is observed between the second impacts with or without removal: removal of the first boulder has little to no effect on the response of the barrier during the second impact. The deflection at the impact point of the second boulder (Fig. 12b) is almost identical in both cases. Tension in the upstream cable S2 (Fig. 12c) and longitudinal cable S8 (Fig. 12d) exhibits a similar behavior. It is also interesting to observe that while the global stiffness of the barrier increases after the first impact (smaller deflection and larger force), it is not necessarily the case for every component locally as tension in upstream cable S2, for example, is lower during the second impact. Differences due to boulder removal do, however, appear in the equilibrium geometry of the barrier after the first impact (Table 4). As expected, removal of the boulder increases the residual height and decreases the residual deflection of the barrier.

Discussion These results tend to indicate that the behavior of barrier A for an energy of 90 kJ is similar if boulder removal is operated or not. This can be explained by two major technological aspects of rockfall barriers.

On the one hand, the energy dissipating devices limit the tension to values around the activation force (Fig. 12d). Limiting tension in the longitudinal cables in turn limits the tension in the entire structure and bounds peak forces for all components. Forces in the barrier, therefore, depend mostly on the current deformed geometry.

On the other hand, flexible rockfall barriers adapt to loading through deformation. The barrier undergoes large deflection during the first impact, but changes in the deformed geometry due to removal of the first boulder in the net are not influential. When removing the first boulder, the barrier recovers at most the increase in gravitational potential energy of the boulder during removal, that is: $\Delta E_p = mg\Delta z = 740\,\text{kg} \times 9.81\,\text{m/s}^2 \times (2.53 - 2.16)\,\text{m} = 2.7\,\text{kJ}$. That value is negligible when compared to the 90 kJ of impact energy: only 3 % of the impact energy of the second boulder is used to re-deform the net in a configuration close to what it would have been should removal had not been performed.

These results may only be valid as long as the energy dissipating devices are functional and can limit forces to reasonable values. If during the second impact one energy dissipating device fails or reaches its stroke, the behavior of the barrier would change drastically and the above mechanical analysis would not hold (Castanon-Jano et al. 2017). Another aspect to be considered is the decrease in residual height. A smaller residual height reduces the number of high trajectory boulders the barrier can intercept. The barrier, therefore, could not catch boulder it would have enough resistance to stop and does not protect targets from those trajectories. As a result, boulder removal appears to be optional when the energy dissipating devices are still in capacity to function properly and when the barrier height is not significantly reduced with respect to the design expectations.

4.2.2 Asymptotic Response under Repeated Impacts

The previous numerical simulations highlighted that for low energies, boulder removal may not be necessary as long as energy dissipating devices are functional. That first conclusion raises questions regarding the behavior

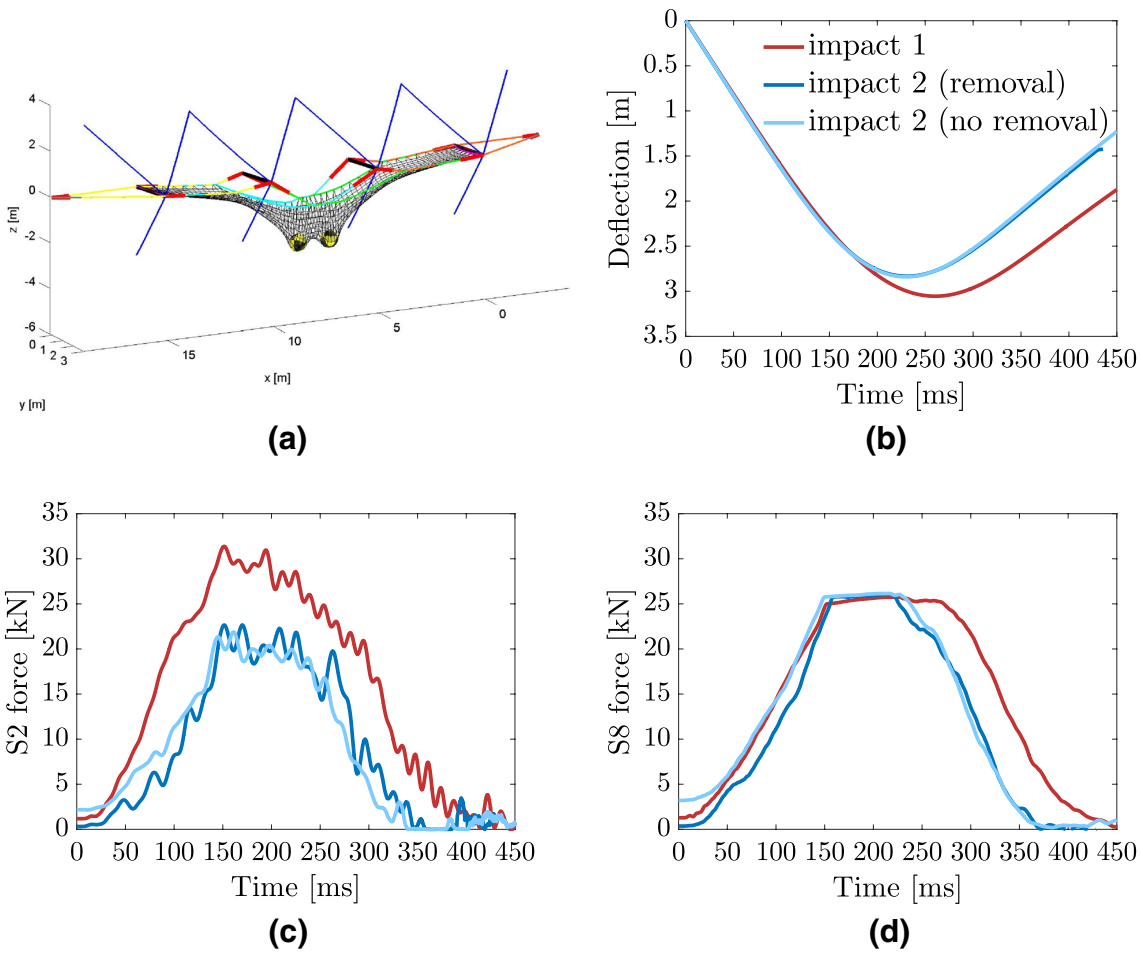

Fig. 12 Simulation of rockfall event: **a** impacted barrier, **b** deflection of the net, **c** force in upstream cable S2, **d** force in longitudinal cable S8

Table 4 Residual deflection and residual height of the barrier after the first impact

Residual dimension	Without removal (m)	With removal (m)
Deflection	2.53	2.16
Height	1.74	1.86

of rockfall barriers subject to a larger number of repeated impacts. Neglecting the purely elastic response, materials and structures under force-controlled cyclic loading may exhibit three main force–displacement behaviors (Lemaitre and Chaboche 1990):

1. elastic shakedown: open cycles with energy dissipation converging toward a non-dissipative closed cycle;
2. plastic shakedown: open cycles with energy dissipation converging toward a stabilized elastoplastic cycle with hysteresis loop;
3. ratcheting: non-converging open cycles with increasing cumulative irreversible deformation leading to failure.

For rockfall barriers, impacts only occur in one direction and there is no reversal of the loading. As a result, there cannot be reversal of plastic deformation and plastic shakedown is not possible. The barrier cyclic response must be either elastic shakedown or ratcheting. The purpose of the present section is to determine the type of asymptotic response of rockfall barriers and to identify the main variables controlling such response.

Simulations and results To conduct this original numerical investigation, barrier A is subject to 15 repeated, identical and consecutive impacts with boulder removal. Impact simulations are performed in the same conditions as the validation single impact test presented in Sect. 3.1 using an impact energy of 90 kJ (impact velocity of 15.6 m/s), one-third of the reference energy level. The stroke of the energy dissipating devices is considered infinite. This assumption is made to prevent failure due to a limitation in the device elongation and permits numerical

study of the asymptotic behavior assuming the devices remain functional over the impacts. Some friction based devices actually use very long cables (several meters) and can be considered to have infinite stroke. This assumption could also be interpreted as a barrier whose maintenance only consists in replacing the energy dissipating devices when the remaining elongation is deemed insufficient, adding indefinite stroke when necessary. Simulation results of the 15 repeated impacts are presented in Fig. 13. The force–displacement relationship of the entire barrier is obtained taking the total vertical force on the boulder (self weight plus net reaction) and the net cumulative elongation. The response shows open loading–unloading cycles whose area decreases and whose increase in total elongation slows down over impact repetitions (Fig. 13a). Due to the dynamic impact loading, the results reported in Fig. 13a do not correspond to equilibrium configurations. A non dissipative impact could result in an open cycle of force–displacement as some of the impact energy is not restored to the boulder and remains in the barrier as kinetic and potential elastic energy (the total mechanical energy of the system composed of the barrier and the boulder would, however, remain constant). Therefore, distinction between elastic shakedown or ratcheting cannot be solely based on the force–displacement response of the boulder alone. The residual height of the barrier (Fig. 13b) decreases with the number of impacts. There is a sharp decrease during the first seven impacts followed by a much more moderate one that almost tends to a stabilized value. The dynamic response of lateral cable S4 is given in Fig. 13c. The first noticeable feature of these curves is the striking difference between the first impact and every other impact in terms of loading time. The barrier becomes much stiffer after the first impact and stiffness increases slowly after that. A non impacted structure is very different from a previously impacted one and that difference is greater than between two structures previously impacted a different amount of times. The second noticeable feature of these curves is the apparent convergence toward one given response. The responses for the last few impacts are almost indiscernible. The force–elongation response of energy dissipating device LL1 (cable S7) is given in Fig. 13d. It can be seen that elongation keeps increasing until the last impact. As the activation force of the energy dissipating devices bounds tensions in the structure (Fig. 13c), elongation of the energy dissipating device seems the most reliable measurement to assess the asymptotic behavior of the barrier. Device LL1 is stressed beyond the activation force during each impact: for that given energy of 90 kJ, barrier A has not reached elastic shakedown behavior after 15 impacts and may be undergoing ratcheting.

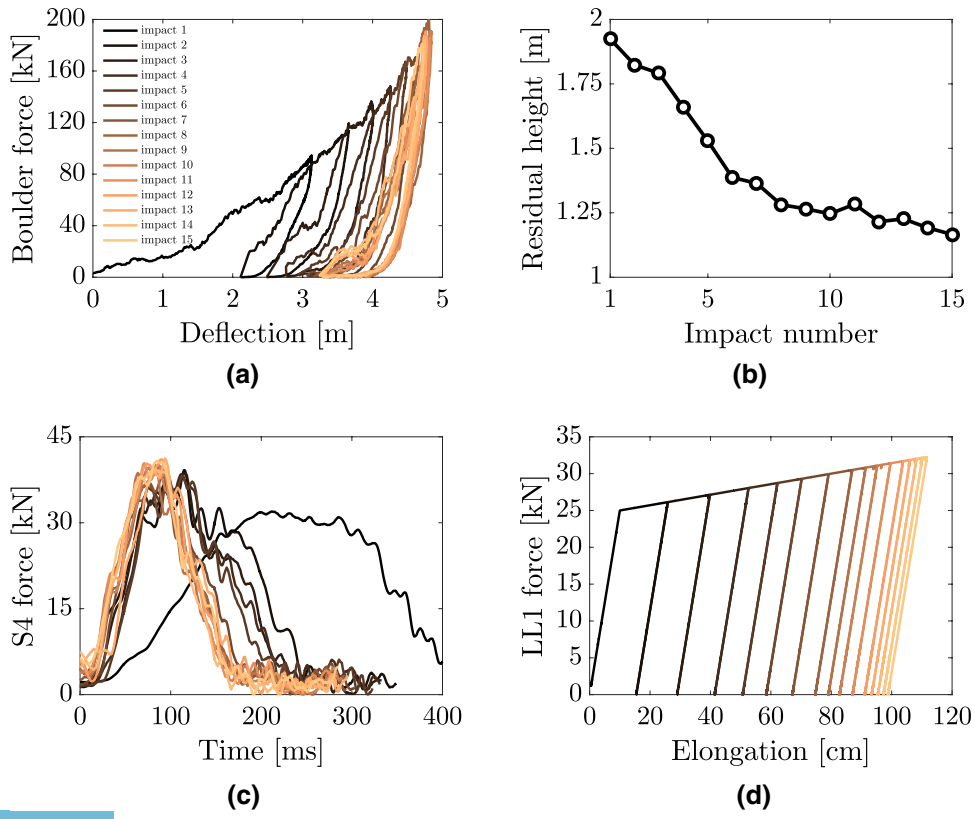

Fig. 13 Asymptotic response of barrier A: **a** force–deflection response of the barrier, **b** residual height of the barrier, **c** force in lateral cable S4, **d** force–elongation response of energy dissipating device LL1

5 Discussion

Depending on the impact energy and the activation force of the energy dissipating devices, rockfall barriers under repeated identical impacts can exhibit either elastic shakedown or ratcheting. For a given impact energy,

- if tensions generated in the energy dissipating devices are lower than the activation force, only limited energy dissipation would occur through friction and yielding in the net and the barrier can be considered to have reached a state of elastic shakedown;
- If tensions greater than the activation force are needed to stop the boulder, the energy dissipating devices would be activated during every impact and the total plastic deformation would keep increasing, causing ratcheting.

Therefore, for a given barrier there is a limit state, defined by pairs of impact energy E_c and activation force F_y, separating the asymptotic response of the barrier between elastic shakedown and ratcheting. Let us define the shakedown criterion as the ratio of the maximum elongation reached by an energy dissipating device to the elongation necessary to activate the dissipation mechanism. If the shakedown criterion is smaller than 1, the device is not activated; if the criterion is larger than 1, the device is activated. The shakedown criterion for the 12 interior dissipating devices over the 15 repeated impacts is presented in Fig. 14a. Elastic shakedown is achieved if and only if none of the energy dissipating device are activated during an impact; the shakedown criterion for the entire barrier can, therefore, be defined as the maximum value of that criterion among all the energy dissipating devices. If that maximum shakedown criterion is larger than 1, the barrier undergoes ratcheting; if it is smaller than 1, the barrier undergoes elastic shakedown. Determination of the shakedown behavior for barrier A has been performed for a range of activation forces F_y and impact energy E_c using a dichotomy method; the resulting phase diagram is presented in Fig. 14b. It should be noticed that each data point in Fig. 14b represents a simulation of 15 repeated impacts. This computationally expensive numerical campaign has been performed in about 10 hours of calculation time using Single Instruction Multiple Data (SIMD) parallel simulations on a cluster of Intel Xeon E5-2670 2.60 GHz 16-core CPUs. The limit state between elastic shakedown and ratcheting is approximated by a cubic polynomial. The studied case ($E_c = 90$ kJ, $F_y = 25$ kN) lies far from the limit state, in the ratcheting phase, confirming our previous qualitative observations. The value of the maximum shakedown criterion for that case after 15 impacts is 1.0252. Even though the barrier would undergo ratcheting due to an exponential increase in its energy dissipating device's elongation, the relatively moderate value of that exponential base would allow the structure to undergo a reasonable amount of impacts before the elongation reaches the stroke of the energy dissipating device. As a matter of fact, with an exponential increase of 2.52 % in elongation during each impact, an additional 15 impacts would increase the current elongation by 45 %. Given the natural frequency of impacts in situ, a barrier lying in the ratcheting domain might still be used without a major risk of failure due to a lack of stroke before performing maintenance. Failure may still occur due to other causes such as fracture of cables, rings, anchors or buckling of posts and is checked for after the simulation is complete. The ultimate strength of anchors strongly depends on the soil properties and cannot be given a priori. The maximum axial force in the posts P1–P4 obtained numerically for all 15 impacts is, respectively, 110 kN, 59 kN, 59 kN and 105 kN, largely below the critical buckling load. The maximum tension in all cables is 43 kN, below the ultimate strength of 96 kN of the least resistant cable of the structure. The most stressed rings are those located in the impact zone.

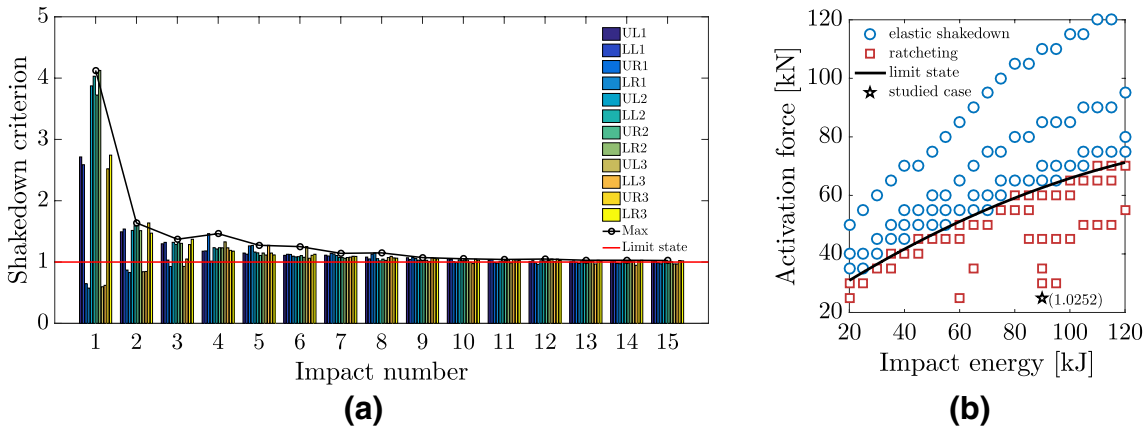

Fig. 14 Shakedown behavior of barrier A: **a** shakedown criterion for $F_y = 25$ kN and $E_c = 90$ kJ, **b** shakedown phase diagram

Over the 15 impacts, the maximum tension in the perimeter linkage of any ring of the net reaches 21.7 kN, below the ultimate tension along the perimeter estimated at 23.3 kN. Therefore, from the available numerical and experimental data, no element in the structure reaches failure over the course of the 15 impact simulations. Nevertheless, complex damage and fatigue processes occurring in the components cannot be fully accounted for with the present models which are not formulated at the local material scale and it is important to be aware of the limitations of the simple structural failure criteria used in the present analysis. Additional caution is advised in the estimation of the protection capacity for actual rockfall barrier management and applications.

5.1 Stochastic investigation of structural variability

In this section, the performances of the models and their implementation are taken advantage of. Thanks to the low computational cost of the simulations, it is possible to perform stochastic analyses that require computation-intensive methods. Several structural reliability studies have been performed on rockfall barriers in order to asses their efficacy under realistic rockfall events, e.g. (Mentani et al. 2016b, a; Bourrier et al. 2015; Toe et al. 2018). In these studies, the response of a deterministic barrier model under impacts of variable kinematics is investigated. As highlighted by the experimental full-scale tests on barrier A presented in Sect. 3.1, the structure itself can exhibit variability and, as a result, the experimental global response of the barriers subject to identical loading conditions may differ noticeably. In the sequel, structural reliability is investigated considering variability in the barrier structural components only. This novel approach permits evaluation of the variability of the barrier performances under a deterministic loading condition as opposed to the more classical study of a deterministic barrier model under variable loading conditions.

The purpose of this stochastic investigation was to determine and quantify how the known input variability in some structural components influences the response of the barrier and affects its output performances. In the present study, the activation forces $\mathbf{A} = (F_{y_1}, \ldots, F_{y_n})$ of the n energy dissipating devices are chosen as variable input parameters. The influence of the variability in the activation forces is studied through an output quantity $R(\mathbf{A})$. For demonstration purposes, the height ratio $R = \text{minimum height}/\text{nominal height}$ is studied as the sought quantity. The minimum height is the smallest height measured during the impact and the nominal height is the initial height. This definition purposely resembles the ETAG 27 residual height criterion evaluated during the SEL test. Minimum height differs, however, from the residual height, but is preferred in this study since it does not require the expensive computation of the equilibrium configuration after impact. The activation forces of the devices are considered as components of the random vector $\mathbf{A}$ of given multivariate joint probability density function (PDF) f_{A}. Knowing f_{A}, the aim of this study was to determine the probability density function f_R of the scalar random variable $R(\mathbf{A})$. Given the complex non-linear behavior of the rockfall barrier and its corresponding numerical model, it is not possible to obtain a closed-form expression of the PDF of R in terms of that of $\mathbf{A}$. Instead, stochastic methodologies are used in order to either determine the value of a given deficiency probability $P_{\mathrm{f}} = P(R < r)$ for a given threshold r or to define an approximation of the PDF of the random variable R.

In this study, two methods based on these two methodologies are applied to barrier A to evaluate its behavior under variability in the energy dissipating devices' behavior. First, a surface response method (FORM) is used to perform sensitivity analysis to determine the most influential devices and to evaluate a given deficiency probability. Second, a metamodel, using polynomial expansion is defined to approximate the density function of the height ratio.

5.1.1 Limit State FORM

The FORM is applied to the barrier A model. Activation forces of the devices are assumed to be independent normal random variables of parameters $\mu_{F_y} = 25\,\text{kN}$ and $\sigma_{F_y} = 2\,\text{kN}$. Given the limited activation of the external energy dissipating devices observed in Fig. 11b, only the 12 internal devices are considered as input variables. As the limit state is unknown, it is estimated by means of numerical simulations with the GENEROCK software. The FORM limit state is obtained using an axial design of experiments and the Rackwitz algorithm. For a given height ratio threshold r, the method consists in finding the design point $\mathbf{x}^*$ defined as the most likely set of input variables (activation forces) to verify $R = r$. The FORM deficiency probability is then estimated by $P_{\mathrm{f}}^{\mathrm{FORM}} = P(R < r) \approx \Phi(-\|\mathbf{x}^*\|)$ where Φ represents the cumulative distribution function of the standard normal distribution. For an arbitrary value of $r = 0.57$, convergence is obtained after 3 iterations, requiring 75 impact simulations and the FORM deficiency probability is estimated at $P_{\mathrm{f}}^{\mathrm{FORM}}(r = 0.57) = 0.0314$. For each input variable A_i, the importance factor gives the influence of that variable on the performance function: the larger the importance factor, the more influential the input variable in the performance. The importance factor can be defined as $\alpha_i^2 = x_i^{*2}/(\mathbf{x}^* \cdot \mathbf{x}^*)$ and is given for the 12 interior energy dissipating devices in Table 5. The results confirm previous observations that the most influential dissipating devices in the response are those with the largest elongation: the devices of the central module LL2, LR2, UL2 and UR2 and those of the lateral modules

Table 5 Importance factor of the energy dissipating devices of barrier A

Upper devices						
Identifier	UL1	UR1	UL2	UR2	UL3	UR3
Importance factor	0.0194	0	0.2843	0.1608	0	0.0053
Lower devices						
Importance factor	0.0092	0	0.0476	0.4645	0	0.0088
Identifier	LL1	LR1	LL2	LR2	LL3	LR3

Table 6 Parameters for generating the metamodels

Input	C1	C2
Number of devices	8	4
Polynomial degree	4	4
Number of simulations	1500	300

attached to them, respectively, LR3, LL1, UR3 and UL1. It is also interesting to notice that the inner devices of the lateral modules (LR1, UR1, LL3 and UL3) showed little to no elongation and have no influence on the studied performance of barrier A. The relative importance of the devices only hold for a centered impact and would differ should the location of the impact be modified.

5.1.2 Metamodel Polynomial Expansion

In this second investigation, a metamodel is used to approximate the output quantity and to obtain an estimate of its entire density functions at a lower calculation cost. A Latin Hypercube Sampling (LHS) is taken as the design of experiments to build the meta-model using a fourth-order Hermite polynomial approximation.

The analysis is limited to two configurations: configuration C1 with the eight influential internal energy dissipating devices (UL1, LL1, UL2, LL2, UR2, LR2, UR3 and LR3) as input variables and configuration C2 with only the four central energy dissipating devices (UL2, LL2, UR2 and LR2). Information about the different metamodel configurations are gathered in Table 6. Once the least-squares regression on simulation results has been performed to generate the metamodel, the cumulative frequency is obtained by a Monte Carlo simulation of 200,000 trials. Cumulative frequency for the two configurations is presented in Fig. 15. This method provides a global approximation of the entire cumulative distribution function of the height ratio through least-squares regression while the FORM provides one particular value of the deficiency probability and identifies the most influential input variables from local exploration of the limit state. It is interesting to notice that differences in the deficiency probabilities are rather large between the different metamodel configurations. In configuration C2, devices UL1, LL1, UR3 and LR3 have a deterministic activation force of 25 kN

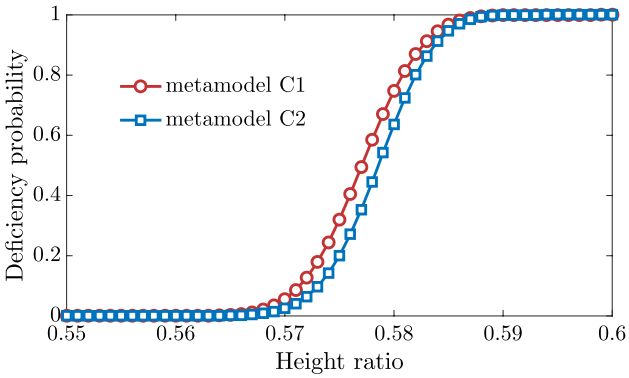

Fig. 15 Cumulative distributions obtained by polynomial expansion metamodels

while those values vary and can be lower in configuration C1. Given that each of these devices is attached in series to one of the central devices, respectively, UR2, LR2, UL2 and LL2, by one longitudinal cable, the force exerted by a longitudinal cable to activate one of the devices is the smallest activation force of the two devices. That may explain why the height ratio in configuration C1 is more likely to be low than in configuration C2. The metamodel response also depends on the number of data points in the design of experiments and the degree of the polynomial approximation. That can in part explain the differences observed between C1 and C2 (Fig. 15). Finally, metamodels provide an overall optimal approximation of the surface response that may not be optimal in the sought regions of small probabilities. For the height ratio threshold $r = 0.57$, the deficiency probabilities given by the FORM is $P_{\mathrm{f}}^{\mathrm{FORM}} = 0.0314$ while those given by the metamodels are $P_{\mathrm{f}}^{C1} = 0.051$ and $P_{\mathrm{f}}^{C2} = 0.0252$.

6 Conclusion

In this article, the GENEROCK rockfall barrier modeling software is introduced. Its underlying principles and capabilities are presented and discussed. Validation and exploratory simulations are performed to highlight the capacity of the generic approach to answer scientific, regulatory and operational research problems. In particular, the mechanical

models of two barriers of distinct technology are introduced and validated against experimental data from full-scale impact tests. Specific advances in mechanical modeling, namely accounting for the irreversible behavior of ring nets and for the curtain effect, as well as low computational cost, make the present developed models well designed and their numerical implementation effective in addressing the complex nonlinear behavior of rockfall barriers.

The influence of the curtain effect first shows the importance of properly accounting for this phenomenon in the modeling to track the barrier response. Large variations in the stiffness and deformed geometry of the structure, elongation of energy dissipating devices and tension in cables have been identified using different modeling assumptions. Simulation results accounting for the curtain effect using the proposed sliding cable model compared best with experimental data. Repeated impacts on the barrier are investigated afterwards and show the capabilities of the ring net and barrier models to cope with realistic and complex loading cases, accounting for the accumulation of irreversible deformation. The limited influence of boulder removal on the barrier response suggests barrier clearing operations may be carried out less frequently without lowering the protection capacities of the structure. Numerical exploration of the asymptotic behavior of rockfall barriers also indicates that in some specific conditions, their retaining capacity may remain important over a very high number of impacts and without maintenance. Such novel information can have direct practical consequences on current rockfall barriers' management practices. Eventually, stochastic investigation is conducted and permits determination of deficiency probability concerning the height of the barrier. This study is based on variability in the structural properties of the barrier as opposed to the more classical study of the variability in the loading. Most generally, this investigation highlights the computational capabilities of the present work to tackle regulatory problems by means of computation-intensive methods.

The results of the exploratory investigations presented are mostly obtained from numerical simulations on one barrier model. It should be noted that some of the results may be specific to that given technology of barriers. However, implementation of additional models describing different barrier technologies in the GENEROCK software is required and the main conclusions drawn in this manuscript are expected to remain valid regardless of the investigated barrier technological details. The computational approach presented is already effective in addressing a range of research problem for the currently available barrier models. Future work will pursue the implementation of component models (deformable posts, chain-link nets...) and the developments presented in this article to offer additional numerical insight into the scientific, regulatory and operational research problems identified.

Acknowledgements The authors would like to express their sincere thanks to the French National Project C2ROP (Chutes de Blocs, Risques Rocheux et Ouvrages de Protection, www.c2rop.fr) for having supported this work and for fostering the development of the GENEROCK software potential applications.

References

Andrew RD, Fry DA, Bookwalter RE (1998) Field testing and evaluation of various rock fall control system. Chama ValleyProductions, LLC, Chama Valley

Arpin BD (2013) Development of standardized testing procedures for flexible rockfall fence systems. Master's thesis, Colorado School of Mines, Golden

Bertrand D, Trad A, Limam A, Silvani C (2012) Full-scale dynamic analysis of an innovative rockfall fence under impact using the discrete element method: from the local scale to the structure scale. Rock Mech Rock Eng 45(5):885–900

Bourrier F, Lambert S, Baroth J (2015) A reliability-based approach for the design of rockfall protection fences. Rock Mech Rock Eng 48(1):247–259

CAN (2018) Travaux spéciaux: accès difficile, risques naturels, maritime et fluvial. CAN - Le Relut, 26270 Mirmande, France. http://www.can.fr. Accessed 4 June 2019

Castanon-Jano L, Blanco-Fernandez E, Castro-Fresno D, Ballester-Muñoz F (2017) Energy dissipating devices in falling rock protection barriers. Rock Mech Rock Eng 50(3):603–619

Castanon-Jano L, Blanco-Fernandez E, Castro-Fresno D, Ferreño D (2018) Use of explicit fem models for the structural and parametrical analysis of rockfall protection barriers. Eng Struct 166:212–226. https://doi.org/10.1016/j.engstruct.2018.03.064

Cazzani A, Mongiovì L, Frenez T (2002) Dynamic finite element analysis of interceptive devices for falling rocks. Int J Rock Mech Mining Sci 39:303–321

Chanut MA, Dubois L, Matot B, Nicot F (2012) Comportement dynamique des écrans de filets sous impact: un modèle générique d'écrans. In: Journées Nationales de Géotechnique et de Géologie de l'Ingénieur, JNGG, Bordeaux, France, 4–6 July

Chanut MA, Coulibaly JB, Lambert S, Nicot F (2018) Numerical investigation of rockfall barrier under realistic on-site impacts. In: International symposium rock slope stability 2018. 13–15 November, Chambery, France. https://www.c2rop.fr/wp-content/uploads/2018/12/RSS2018_proceedings.pdf. Accessed 4 June 2019

Coulibaly JB (2017) Modélisation numérique discrète du comportement mécanique sous impact des structures d'écrans de filets pare-pierres. PhD thesis, University Grenoble-Alpes, Grenoble, France **(in French)**

Coulibaly JB, Chanut MA, Lambert S, Nicot F (2017a) Nonlinear discrete mechanical model of steel rings. J Eng Mech 143(9):04017087

Coulibaly JB, Chanut MA, Galandrin C, Olmedo I, Lambert S, Nicot F (2017b) Generic modeling of flexible rockfall barriers: from components characterization to full-scale numerical simulations. In: 6th Interdisciplinary workshop on rockfall protection, RocExs 2017, Barcelona, Spain, 22–24 May. ISBN: 978-84-946909-4-5

Coulibaly JB, Chanut MA, Lambert S, Nicot F (2018) Sliding cable modeling: An attempt at a unified formulation. Int J Solids Struct 130–131:1–10

de Miranda S, Gentilini C, Gottardi G, Govoni L, Mentani A, Ubertini F (2015) Virtual testing of existing semi-rigid rockfall protection

barriers. Eng Struct 85:83–94. https://doi.org/10.1016/j.engstruct.2014.12.022
Duffy JD, Haller B (1993) Field tests of flexible rockfall barriers. In: Conference on transportation facilities through difficult terrain, Aspen-Snowmass, CO, USA, 8–10 August. pp 465–473. ISBN: 90-5410-343-4
EOTA (2013) ETAG 27—Guideline for European technical approval of falling rock protection kits. European organization for technical approvals. Brussels
Erhart T (2012) Pulley mechanism for muscle or tendon movements along bones and around joints. In: LS-DYNA forum, DYNAmore, Ulm, Germany, 9–10 October. https://www.dynamore.se/en/resources/papers/ls-dyna-forum-2012/documents/passive-3-3. Accessed 4 June 2019
Escallón J, Wendeler C, Chatzi E, Bartelt P (2014) Parameter identification of rockfall protection barrier components through an inverse formulation. Eng Struct 77:1–16
Escallón JP, Wendeler C (2013) Numerical simulations of quasi-static and rockfall impact tests of ultra-high strength steel wire-ring nets using abaqus/explicit. In: 2013 SIMULIA community conference, Vienna, Austria, 23–24 May. https://www.3ds.com/fileadmin/PRODUCTS/SIMULIA/PDF/scc-papers/numerical-simulation-quasi-static-and-rockfall-impact-13.pdf. Accessed 4 June 2019
Escallón JP, Boetticher V, Wendeler C, Chatzi E, Bartelt P (2015) Mechanics of chain-link wire nets with loose connections. Eng Struct 101:68–87
Gentilini C, Govoni L, de Miranda S, Gottardi G, Ubertini F (2012) Three-dimensional numerical modelling of falling rock protection barriers. Comput Geotech 44:58–72
Gentilini C, Gottardi G, Govoni L, Mentani A, Ubertini F (2013) Design of falling rock protection barriers using numerical models. Eng Struct 50:96–106. https://doi.org/10.1016/j.engstruct.2012.07.008
Gerber W, Böll A (2006) Type-testing of rockfall barriers—comparative results. In: International symposium interpraevent, Munich, Germany, 3–4 April, pp 189–198. http://www.interpraevent.at/palm-cms/upload_files/Publikationen/Tagungsbeitraege/2006_1_189.pdf. Accessed 4 June 2019
Gerber W, Grassl H, Böll A, Ammann W (2001) Flexible rockfall barriers—development, standardisation and type-testing in switzerland. In: International Conference on Landslides—causes, impacts and countermeasures. Davos, Switzerland, pp 515–524
Gottardi G, Govoni L (2010) Full-scale modelling of falling rock protection barriers. Rock Mech Rock Eng 43:261–274
Grassl H (2002) Experimentelle und numerische modellierung des dynamischen tragund verformungsverhaltens von hochflexiblen schutzsystemen gegen steinschlag. PhD Thesis, ETH Zurich, Zurich
Grassl H, Volkwein A, Anderheggen E, Ammann J (2002) Steel-net rockfall protection—experimental and numerical simulation. WIT Trans Built Environ 63:11
Hambleton JP, Buzzi O, Giacomini A, Spadari M, Sloan SW (2013) Perforation of flexible rockfall barriers by normal block impact. Rock Mech Rock Eng 46(3):515–526
Heiss C (2004) Characteristics of the testing of rock fall protection kits on transversal test sites on example "Steirischer Erzberg". In: International Symposium Interpraevent, Riva del Garda, Italy, pp 49–58
Hincz K (2009) Nonlinear analysis of cable net structures suspended from arches with block and tackle suspension system, taking into account the friction of the pulleys. Int J Space Struct 24(3):143–152
Lambert S, Nicot F (eds) (2011) Rockfall engineering. Wiley, New York
Lemaitre J, Chaboche JL (1990) Mechanics of solid materials. Cambridge University Press, Cambridge. https://doi.org/10.1017/CBO9781139167970
Luciani A, Todaro C, Peila D (2017) Maintenance and risk management of rockfall protection net fences through numerical study of damage influence. Frattura ed Integrità Strutturale 12(43):241–250. https://doi.org/10.3221/IGF-ESIS.43.19
McCauley MT, Works BW, Naramore SA (1985) Rockfall Mitigation. California Department of Transportation, Sacramento
Mentani A, Giacomini A, Buzzi O, Govoni L, Gottardi G, Fityus S (2016a) Numerical modelling of a low-energy rockfall barrier: new insight into the bullet effect. Rock Mech Rock Eng 49(4):1247–1262. https://doi.org/10.1007/s00603-015-0803-1
Mentani A, Govoni L, Gottardi G, Lambert S, Bourrier F, Toe D (2016b) A new approach to evaluate the effectiveness of rockfall barriers. Procedia Eng 158:398–403. https://doi.org/10.1016/j.proeng.2016.08.462. VI Italian conference of researchers in geotechnical engineering, CNRIG2016—Geotechnical engineering in multidisciplinary research: from microscale to regional scale, Bologna, Italy, 22–23 September 2016
Mentani A, Govoni L, Giacomini A, Gottardi G, Buzzi O (2018) An equivalent continuum approach to efficiently model the response of steel wire meshes to rockfall impacts. Rock Mech Rock Eng. https://doi.org/10.1007/s00603-018-1490-5
Moon T, Oh J, Mun B (2014) Practical design of rockfall catchfence at urban area from a numerical analysis approach. Eng Geol 172:41–56
Muraishi H, Sano S (1999) Full-scale rockfall test of ring net barrier and components. In: Seminar on Rockfall Tests and Standardization, Davos, Switzerland
Muraishi H, Samizo M, Sugiyama T (2005) Development of a flexible low-energy rockfall protection fence. Q Rep Railway Tech Res Inst 46(3):161–166
Nicot F, Cambou B, Mazzoleni G (2001a) Design of rockfall restraining nets from a discrete element modelling. Rock Mech Rock Eng 34(2):99–118
Nicot F, Cambou B, Mazzoleni G (2001b) From a constitutive modelling of metallic rings to the design of rockfall restraining nets. Int J Numer Anal Methods Geomech 25(1):49–70
Olmedo I, Robit P, Bertrand D, Galandrin C, Coulibaly JB, Chanut MA (2017) Extended experimental studies on rockfall flexible fences. In: RocExs 2017—6th Interdisciplinary Workshop on Rockfall Protection
Peila D, Pelizza S, Sassudelli F (1998) Evaluation of behavior of rockfall restraining nets by full scale tests. Rock Mech Rock Eng 31(1):1–24
Smith DD, Duffy JD (1990) Field tests and evaluation of rockfall restraining nets. Tech. rep., California Department of Transportation, Sacramento, California (USA), cA/TL-90/05
Spadari M, Giacomini A, Buzzi O, Hambleton JP (2012) Prediction of the bullet effect for rockfall barriers: a scaling approach. Rock Mech Rock Eng 45(2):131–144
Toe D, Mentani A, Govoni L, Bourrier F, Gottardi G, Lambert S (2018) Introducing meta-models for a more efficient hazard mitigation strategy with rockfall protection barriers. Rock Mech Rock Eng 51(4):1097–1109. https://doi.org/10.1007/s00603-017-1394-9
Tran PV, Maegawa K, Fukada S (2013) Experiments and dynamic finite element analysis of a wire-rope rockfall protective fence. Rock Mech Rock Eng 46(5):1183–1198. https://doi.org/10.1007/s00603-012-0340-0
Volkwein A (2004) Numerische simulation von flexiblen steinschlagschutzsystemen. PhD thesis, ETH Zurich, Zurich
Volkwein A (2005) Numerical simulation of flexible rockfall protection systems. In: International conference on computing in civil engineering, ASCE, Cancun, Mexico, 12–15 July. https://doi.org/10.1061/40794(179)122
Volkwein A, Schellenberg K, Labiouse V, Agliardi F, Berger F, Bourrier F, Dorren LKA, Gerber W, Jaboyedoff M (2011) Rockfall characterisation and structural protection—a review. Nat Hazards Earth Syst Sci 11(9):2617–2651. https://doi.org/10.5194/nhess-11-2617-2011
Zhou B, Accorsi ML, Leonard JW (2004) Finite element formulation for modeling sliding cable elements. Comput Struct 82(2–3):271–280